HHS Public Access

Author manuscript

Acta Biomater. Author manuscript; available in PMC 2020 October 01.

Published in final edited form as:

Acta Biomater. 2019 October 01; 97: 409–419. doi:10.1016/j.actbio.2019.08.016.

Controlled delivery of basic fibroblast growth factor (bFGF) using acoustic droplet vaporization stimulates endothelial network formation

Xiaoxiao Dong[a,b], **Xiaofang Lu**[b], **Kailee Kingston**[b], **Emily Brewer**[b], **Benjamin A. Juliar**[c], **Oliver D. Kripfgans**[b,c,d], **J. Brian Fowlkes**[b,c,d], **Renny T. Franceschi**[c,e,f], **Andrew J. Putnam**[c], **Zheng Liu**[a], **Mario L. Fabiilli**[b,c,d]

[a]Department of Ultrasound, the Second Affiliated Hospital of Army Medical University, Chongqing, China

[b]Department of Radiology, University of Michigan Health System, Ann Arbor, MI USA

[c]Department of Biomedical Engineering, University of Michigan, Ann Arbor, MI USA

[d]Applied Physics Program, University of Michigan, Ann Arbor, MI USA

[e]Department of Periodontics and Oral Medicine, School of Dentistry, University of Michigan, Ann Arbor, MI USA

[f]Department of Biological Chemistry, University of Michigan Medical School, Ann Arbor, MI USA

Abstract

The challenge of translating pro-angiogenic growth factors for therapeutic purposes has stimulated a myriad of biomaterials-based, delivery approaches. Many techniques rely on incorporating a growth factor into a hydrogel. The kinetics of release can be tuned based on the physiochemical properties of the growth factor and scaffold. We have developed an acoustically-responsive scaffold (ARS), whereby release of a growth factor is non-invasively and spatiotemporally controlled in an on-demand manner using focused ultrasound. An ARS consists of a fibrin matrix doped with a growth factor-loaded, sonosensitive emulsion. In this study, we used an ARS to investigate the impact of basic fibroblast growth factor (bFGF) release on endothelial tubule formation. The co-culture model of angiogenic sprouting consisted of endothelial cell-coated microbeads and dispersed fibroblasts. bFGF release correlated with the acoustic pressure applied while sprout length correlated with both the volume of bFGF-loaded emulsion in the ARS and acoustic pressure. Minimal bFGF release and sprouting were observed in the absence of ultrasound exposure. Staggering the release of bFGF via multiple ultrasound exposures did not affect sprouting. Additionally, sprouting did not display a dependence on the distance between

Corresponding Author: Mario Fabiilli, Ph.D., University of Michigan, 3226A Medical Sciences Building I, 1301 Catherine Street, Ann Arbor, MI 48109-5667, Phone: 734-647-9326, mfabiill@umich.edu; Zheng Liu, M.D., Ph.D., Army Medical University, The Second Affiliated Hospital, 183 Xinqiao Street, Shapingba District, Chongqing 400037, Phone: 023-68755660, liuzhengs@hotmail.com.

each microbead and the ARS. Overall, these results highlight the potential of using ultrasound to control regenerative processes via the controlled delivery of a growth factor.

Graphical Abstract

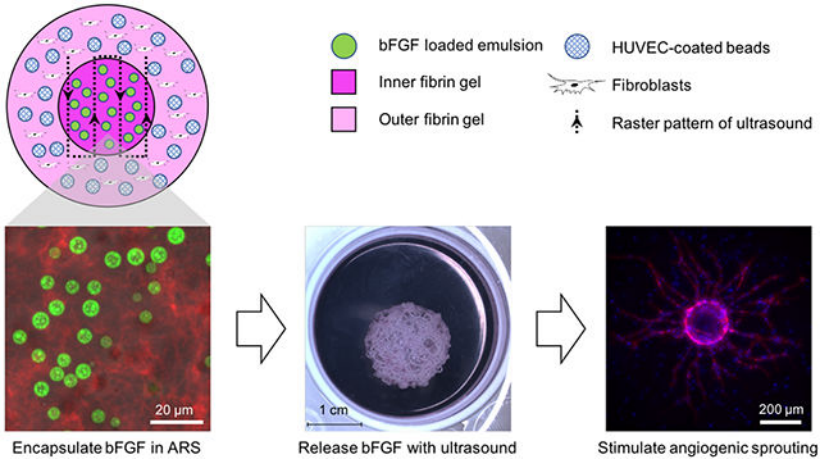

Keywords

ultrasound; controlled release; drug delivery; endothelial cells; fibrin; acoustic droplet vaporization; angiogenesis

1. Introduction

Blood vessel formation is a crucial process in the development, homeostasis, and regeneration of most types of tissue. The stimulation of vascularization is being studied for the treatment of ischemic cardiovascular diseases and to improve the viability of engineered tissue substitutes upon *in vivo* implantation. One technique being extensively explored is the administration of pro-angiogenic molecules, such as growth factors (GFs) or genetic vectors encoding for GFs, to stimulate vessel growth. In the context of cardiovascular disease, this technique has been termed therapeutic angiogenesis [1], with the intended goal of increasing collateral vessel formation to circumvent pre-existing vasculature with impaired flow. In preclinical studies, experiments using pro-angiogenic factors like basic fibroblast growth factor (bFGF) have demonstrated efficacy in treating models of coronary artery [2, 3] and peripheral artery diseases [4, 5]. Numerous clinical studies have evaluated the effects of bFGF, as well as other GFs, in patients with coronary artery [6, 7] and peripheral artery [8–11] diseases. To date, however, translation has remained a challenge, with no pro-angiogenic growth factor being yet approved by the United States Food and Drug Administration for the treatment of cardiovascular disease.

The ineffectiveness of injectable solutions of GFs, especially in terms of clinical outcomes, has spurred the development of biomaterials to improve the efficacy of GF-based therapies. Hydrogels are frequently used as matrices for the delivery of GFs, thereby increasing their half-lives, increasing protein stability, and decreasing the rate of enzymatic degradation [12,

13]. Temporal control of GF release is often tuned by modulating scaffold properties as well as exploiting strategies for GF immobilization and/or GF encapsulation. For example, extended release of bFGF, via the use of heparin-conjugated fibrin [14] or incorporation into poly(lactide-co-glycolide) (PLGA) nanospheres [15], yielded greater vessel density *in vivo* relative to scaffolds with burst release. Spatial control of GF presentation is typically generated via the use of anisotropic constructs. For example, gradients of bFGF were generated by incorporating the GF, at different concentrations, into PLGA microspheres which were then incorporated into polycaprolactone fibers; upon implantation, vessel density correlated with the steepness of the bFGF gradient [16].

We have developed a scaffold-based, delivery method for GFs where release is controlled using focused ultrasound (US). Unlike the aforementioned strategies, our method enables non-invasive and spatiotemporally controlled GF release in an on-demand manner. As demonstrated previously, release of a GF or other payload can be modulated after *in vivo* implantation of the scaffold via the application of megahertz-range US [17, 18]. The acoustically-responsive scaffold (ARS) consists of a sonosensitive emulsion embedded within a fibrin matrix. The micron-sized emulsion has a water-in-perfluorocarbon (PFC)-in-water (W_1/PFC/W_2) structure, with the GF or other water-soluble payload to be delivered in the W_1 phase. Release of the GF occurs via a mechanism called acoustic droplet vaporization (ADV) [19], whereby the PFC within each double emulsion droplet phase transitions from a liquid into a gas, thereby disrupting the droplet morphology and causing GF release. ADV is a threshold-based process and as such, the US pressure amplitude must be above the ADV threshold in order for the PFC to be vaporized and the GF to be released. Due to the use of pulsed waveforms (i.e., low duty cycles), ADV is a non-thermal process that is initiated by superharmonic focusing and dependent on the rarefactional component of the US wave [20, 21]. ARSs can be formulated to enable sequential release of two payloads using emulsions with distinct ADV thresholds [22].

In this study, we investigate the impact of bFGF delivery using an ARS on an established, co-culture model of vascular morphogenesis. The model consists of endothelial cells, coated onto microcarrier beads, as well as fibroblasts – both of which are embedded within a fibrin matrix [23, 24]. The inclusion of fibroblasts facilitates tubulogenesis via the secretion of pro-angiogenic factors, which are required for endothelial cell sprouting and lumen formation [25]. Additionally, when co-cultured with fibroblasts, endothelial cells upregulate expression of proteases, which promotes capillary formation [26]. In the absence of stromal cells, endothelial cells can invade the matrix, but do not form capillary-like structures [27].

We used a gel-in-gel construct to study the effects of bFGF delivery, where the inner gel was an ARS and the outer gel contained endothelial cell-coated microbeads and fibroblasts. The monodispersed bFGF-loaded emulsion, contained in the inner gel, was generated using a microfluidic device. We evaluated angiogenic sprouting as a function of US pressure, emulsion loading, and temporal presentation of bFGF. The distribution of bFGF in the *in vitro* system was also quantified. As will be shown, US enables non-invasive control of angiogenic sprouting via the release of bFGF from an ARS.

2. Materials and Methods

2.1 Preparation of the emulsions

The double emulsion (W_1/PFC/W_2) was prepared with perfluoroheptane (PFHep, C_7F_{16}, CAS#: 335-57-9, Sigma-Aldrich, St. Louis, MO, USA) as the PFC phase using a previously published method [18]. A fluorosurfactant copolymer, consisting of Krytox 157 FSH (CAS# 51798-33-5, DuPont, Wilmington, DE, USA) and polyoxyethylene glycol (MW: 1000 g/mol, CAS# 24991-53-5, Alfa Aesar), was dissolved at 2% (w/w) in PFHep. The PFHep solution was combined at 2:1 (v/v) with an aqueous solution of 0.5 mg/mL bFGF (Cat#: GF003AF, EMD Millipore, Temecula, CA, USA) in phosphate buffered saline (PBS, Life Technologies, Grand Island, NY, USA) containing 10 mg/mL bovine serum albumin (Sigma-Aldrich) and 2 μg/mL (i.e., 0.4 U/mL) heparin (Cat#: 375095, Calbiochem, San Diego, CA, USA). Heparin was added to inhibit proteolytic degradation of bFGF [28]. The PFHep and W_1 phases were sonicated (Q55 with CL-188 immersion probe, QSonica, LLC, Newton, CT, USA) for 30 seconds while on ice to minimize heating. The resulting primary emulsion, with a water-in-PFC (W_1/PFC) structure, was pumped at 1 μL/min through an in-line filter (0.5 μm stainless steel frit, Cat# 24993, Restek, Bellefonte, PA, USA) and then into the inner channel of a quartz microfluidic chip (Cat# 3200146, Dolomite, Royston United Kingdom) using a syringe pump (KDS-410, kd Scientific, Holliston, MA, USA). Simultaneously, 50 mg/mL Pluronic F68 (CAS# 9003-11-6, Sigma-Aldrich) in PBS was pumped at 10 μL/min through an inline filter and then into the outer channels of the chip using a second syringe pump (78-0388, kd Scientific). In a subset of the experiments, blank or fluorescent emulsions were prepared as described above with only PBS or PBS containing 1.67 mg/mL Alexa Fluor 488-labeled dextran (MW: 10 kDa, Life Technologies) as the W_1 phases, respectively. The chip was mounted on an inverted microscope (DMIL, Leica Microsystems, Buffalo Grove, IL, USA) which enabled visualization of emulsion production. Emulsions were characterized with a Coulter counter (Multisizer 4, Beckman Coulter, Brea, CA, USA) in the range of 1-30 μm.

2.2 Cell culture

Human umbilical vein endothelial cells (HUVECs, Lonza, Walkersville, MD, USA) were cultured in fully supplemented VascuLife VEGF endothelial cell culture medium (Lifeline Cell Technology, Frederick, MD, USA) and used between passages 1-4. Normal human dermal fibroblasts (NHDFs, Lonza, Walkersville, MD, USA) were cultured in Dulbecco's modified eagle medium (DMEM, Life Technologies, Grand Island, NY, USA) supplemented with 10% (v/v) fetal bovine serum (FBS, Life Technologies), 100 U/mL penicillin, and 100 μg/mL streptomycin (Life Technologies) and used up to passage 4. Media for both cell types were exchanged every 2 days and cells were harvested below 80% confluence with trypsin-EDTA (Life Technologies).

2.3 Construct fabrication

HUVEC-coated microbeads were prepared by modifying a previous method [29, 30]. Cytodex microcarrier beads (C3275, Sigma-Aldrich) were autoclaved in PBS and washed 3 times with VascuLife medium before use. The day before construct assembly, 10^4 beads were combined with 4×10^6 HUVECs in 5 mL of VascuLife medium and agitated every

20-30 min in an upright T-25 culture flask (Corning Inc, Corning, NY, USA). After 4 h, 5 mL of fresh, fully supplemented VascuLife medium was added and the mixture was transferred to a new T-25 flask and incubated overnight in the standard culture position. The following day, beads were transferred from the flask to a 15 mL conical tube (VWR, Radnor, PA, USA) and allowed to settle by gravity following three washes with fresh VascuLife medium. The HUVEC-coated microbeads were ready for use following the triplicate washing.

A summary of all cell experiments is listed in Table 1. To assess the dose response of bFGF concentration on angiogenic sprouting, constructs were prepared in 24-well culture plates (Fisher Scientific, Pittsburgh, PA, USA). Bovine fibrinogen (Sigma-Aldrich) was dissolved at 2.5 mg/mL in DMEM and sterile filtered through a 0.22 μm PES membrane filter (Cat# 6780-2502, Whatman, United Kingdom). The fibrinogen solution was degassed under vacuum prior to use. NHDFs and HUVEC-coated microbeads were added to the fibrinogen solution at final concentrations of 2.5×10^4 cells/mL and 50 beads/mL, respectively. Bovine thrombin (Thrombin-JMI, King Pharmaceuticals, Bristol, TN, USA) was added to the fibrinogen mixture at a final concentration of 2 U/mL. Briefly, 0.5 mL aliquots of the mixture were added to each well and allowed to polymerize for 5 min at room temperature before being transferred to incubate at 37°C for another 25 min. Each gel was then covered with 1 mL overlying media and placed in a standard tissue culture incubator (37°C, 5% carbon dioxide). For the positive control group, the overlying media was fully supplemented VascuLife medium. For all other groups, the overlying medium was complete media consisting of DMEM/F12 (Life Technologies) supplemented with 10% (v/v) FBS, 100 U/mL penicillin, and 100 μg/mL streptomycin. The next day, the overlying medium of the negative control group was changed to starvation medium consisting of DMEM/F12 supplemented with ITS liquid media supplement (i.e., 10 μg/mL insulin, 5 μg/mL transferrin, and 6.7 ng/mL sodium selenite), 100 U/mL penicillin, 100 μg/mL streptomycin, 100 μg/ml ovalbumin (Sigma-Aldrich), 50 μg/ml L-ascorbic acid (Sigma-Aldrich), 1 μg/ml hydrocortisone 21-hemisuccinate sodium salt (Sigma-Aldrich), and 0.75 U/mL heparin. For the other experimental conditions, the overlying medium was changed to starvation medium with the desired concentration (0.1 ng/mL, 1 ng/mL 2 ng/mL, 5 ng/mL, 10 ng/mL or 100 ng/mL) of bFGF. Gels were subsequently cultured for 7 days or 14 days without any further media changes.

To assess the US-triggered delivery of bFGF, gel-in-gel constructs were cast in 6-well HT Bioflex plates (Flexcell International Co., Hillsborough, NC, USA) (Figure 1A). Each inner gel was an ARS (0.4 mL total volume) consisting of 2.5 mg/mL fibrinogen, 2 U/mL of thrombin, and 0.25% or 1% (v/v) blank emulsion or bFGF-loaded emulsion. Each outer gel (1.5 mL total volume) consisted of 2.5 mg/mL fibrinogen, 2 U/mL thrombin, 2.5×10^4 NHDFs/mL, and 50 HUVEC-coated beads/mL. The outer gels were cast after polymerization of the inner gels. Close contact between the inner and outer gels was confirmed via microscopy, and constructs were excluded if there were any gaps (e.g., air bubbles) between the interface of the gels. Following complete polymerization, each gel-in-gel construct was then covered with 4 mL overlying media and placed in an incubator. For the positive control group, the overlying medium was VascuLife medium. For other groups, complete media was used. All groups, except the positive control, were switched to

starvation media the next day. For every set of experiments, positive and negative control groups were included. A sham exposure group (i.e., same volume of emulsion, -US) was also included.

2.4 US exposure

A calibrated, single-element high intensity focused US transducer (2.5 MHz, H-108, f-number = 0.83, focal length = 50 mm, Sonic Concepts Inc., Bothell, WA, USA) was used to generate ADV within the ARSs. The transducer was driven by pulsed waveforms generated using a dual channel function generator (33500B, Agilent Technologies, Santa Clara, CA, USA), amplified by a gated radiofrequency amplifier (GA-2500A Ritec Inc, Warwick, RI, USA), and passed through a matching circuit (H108_3 MN, Sonic Concepts) to reduce the impedance mismatch between the transducer and amplifier. Gating of the carrier waveform was realized using the second channel of the function generator, resulting in a pulsed signal. The pulse length and pulse repetition frequency (PRF) were 5.4 ps (i.e., 13 cycles) and 100 Hz, respectively. All generated and amplified signals were monitored with an oscilloscope (HDO4034, Teledyne LeCroy, Chestnut Ridge, NY, USA).

After the medium overlying the gel-in-gel constructs was exchanged to starvation media, the BioFlex plate containing the constructs was placed in a degassed, 37°C water tank such that only the bottom of the plate was in contact with water. The transducer was positioned under the plate and connected to a three-axis positioning system (Parker Hannifin, Charlotte, NC, USA) controlled by MATLAB (The MathWorks, Natick, MA, USA). To localize the transducer axially with respect to the ARSs, a pulse echo technique was utilized whereby the transducer was driven by a pulser-receiver (5077PR, Olympus, Center Valley, PA, US). The axial focus of the transducer was positioned with respect to reflections from the well bottom and media-air interface.

The ARSs were exposed to US at either 3.3 MPa or 8.8 MPa peak rarefactional pressure (PRP); the former pressure was just above the ADV threshold in the ARS [31] while the latter pressure was close to the maximum output of the transducer. The corresponding peak compressional pressures were 4.3 MPa and 17.2 MPa, respectively. A sham exposure condition (i.e., -US) was also included. For each exposure, the focus of the US transducer was laterally rastered across the ARS (see top view in Figure 1A) at a speed of 5 mm/s with a 0.5 mm spacing between raster lines. Exposures were done by rastering the geometric focus at three axial (i.e., z) planes of 5 mm, 3 mm, and 1 mm above the bottom of the ARS, with exposures completed from the top/distal (i.e., 5 mm) to bottom/proximal (i.e., 1 mm) direction.

Two different studies were conducted. In the first experiment, the effects of the volume fraction of the bFGF-loaded emulsion within the ARS and acoustic pressure of exposure were investigated. The entire ARS was exposed to US and sprouting was assessed 7 days later. In the second experiment, the impact of the temporal presentation of bFGF was investigated (Table 2). On day 1, different subvolumes of the ARSs (i.e., none, half, or complete) were exposed to 8.8 MPa PRP US. At a later time point (i.e., day 4 or day 7), the remaining half of the ARS was exposed to US. Sprouting was measured on day 7, 10, or 13.

2.5 Imaging and analysis of sprouting and NHDF density

Constructs were fixed for 20 min in buffered zinc formalin (Formalde-Fresh, Thermo Fisher Scientific), washed in triplicate with PBS, and stained overnight with rhodamine labeled *Ulex europaeus* agglutin I (UEA-I, Vector Laboratories, Inc., Burlingame, CA, USA). The next day, constructs were washed in triplicate with PBS and stained overnight with 4',6-diamidino-2-phenylindole (DAPI, Thermo Fisher Scientific). Following triplicate washing in PBS, constructs were imaged at low magnification (4×) via fluorescence microscopy (Eclipse TiE, Nikon, Melville, NY, USA) using MetaMorph software (Universal Imaging/Molecular Devices Corporation, Union City, CA, USA). Beads were randomly selected for imaging and excluded if the tubules anastomosed with those of neighboring beads. For each bead, a stack of UEA-I images was acquired with a step size of 18 μm and then converted to a maximum projection (MP) image for subsequent analysis. MP images were analyzed with the Angiogenesis Tube Formation module in MetaMorph software. Tubules were thresholded, segmented, and quantified to generate values of total tubule length per bead. Total tubule length, which is the sum of the entire tubule network, has been used as a metric to quantify the magnitude of vascular morphogenesis [24, 29, 32]. The motorized stage on the microscope enabled the determination of the distance between each bead and the closest point on the outer edge of the ARS.

The NHDF density was determined by acquiring DAPI images in regions of the outer gel where microbeads were absent. The number of NHDF nuclei were thresholded and counted using open-source image processing software (NIH ImageJ, National Institutes of Health, Bethesda, MD, USA) and then averaged.

2.6 Morphology of the constructs

To confirm emulsion and construct morphology, ARSs were prepared with 1% (v/v) emulsion containing Alexa Fluor 488-labeled dextran in the W_1 phase and 62.5 μg/mL Alex Fluor 647 labeled-fibrinogen (Invitrogen, Grand Island, NY, USA) in the fibrin matrix. The mixture was polymerized within a CoverWell imaging chamber (Electron Microscopy Sciences, Hatfield, PA, USA) and mounted onto a glass microscope slide. ARSs were imaged using an inverted confocal microscope (SP5X, Leica Microsystems) at the University of Michigan Microscopy & Image Analysis Laboratory.

To observe gross morphological changes, ARSs containing 0.25% or 1% (v/v) emulsion were imaged 7 days after exposure to sham, 3.3 MPa PRP, or 8.8 MPa PRP US conditions (as described previously). Gels were rinsed briefly in PBS and then imaged *in situ* using a stereoscope (MZ FLIII, Leica, Deerfield, IL, USA).

2.7 Measurement of bFGF release

To measure bFGF release, acellular constructs were cast in 6-well HT Bioflex plates. The inner gels were either ARSs (0.4 mL total volume), with 0.25% or 1% (v/v) bFGF-loaded emulsion, or fibrin containing an equivalent loading of unencapsulated bFGF as in the two ARS conditions. The outer gels contained fibrinogen, DMEM, and thrombin. Following complete polymerization, each construct was covered with 4 mL of complete media and then placed in a tissue culture incubator. The next day, the overlying media was removed and

saved for analysis. The constructs were then covered with 4 mL of starvation media. The ARSs were exposed to –US, US at 3.3 MPa PRP, or US at 8.8 MPa PRP after the media change using the aforementioned exposure conditions. The overlying media were sampled daily by collecting 0.1 mL of the media for 8 days, including immediately after US exposure. The plates were placed in an incubator throughout the duration of the experiment. In a subset of the constructs, on day 2 or day 8, the outer gels were biopsied (∅: 6 mm, Miltex, York, PA, USA) and digested by adding 0.05 U of plasmin (Sigma-Aldrich) to the biopsied samples. Constructs were only biopsied on one time point and following biopsy, the overlying medium was no longer sampled. The concentration of bFGF in the collected samples was measured using an enzyme-linked immunosorbent assay (ELISA) (DY233, R&D System, Inc., Minneapolis, MN, USA).

2.8 Statistics

Statistical analyses were performed using GraphPad Prism software (GraphPad Software, Inc., La Jolla, CA, USA). The number of independent replicates is listed in the caption for each figure. Significant differences between groups were determined using a one-way ANOVA followed by Tukey's multiple comparisons test, with a significance level of 0.05. A four-parameter logistic function was used to fit tubule length as a function of bFGF concentration where the following parameters are reported: maximum total tubule length (L_{max}), minimum total tubule length (L_{min}), and the bFGF concentration at which half of the maximum total tubule length was observed (C_{50}). A first-order exponential model was used to fit the bFGF release data; the percentage of bFGF released at infinite time (C_{max}) and rate constant (K) are reported. The 95% confidence interval of calculated parameters are listed in the format S [S_L, S_H] where S is the average value, S_L is the lower bound value, and S_H is the upper bound value. A linear model was used in the analysis of total tubule length as a function of bead distance from the ARS.

3. Results

3.1 bFGF stimulates endothelial sprouting

Example MP images of endothelial sprouting, including a segmented image, are shown in Figure 2. Sprouts emanated from the HUVEC-coated microbeads, which were embedded in a fibrin hydrogel containing NHDFs. As seen in Figure 3A, quantification of the UEA-I stained images revealed a sigmoidal relationship between total tubule length and bFGF concentration. bFGF concentrations of 2 ng/mL and higher yielded sprouting that was significantly greater than 0.1 ng/mL, the lowest bFGF concentration. bFGF concentrations of 10 ng/mL and 100 ng/mL yielded significantly greater sprouting on day 14 compared to day 7. The C_{50} on day 14, 5.9 ng/mL [4.7, 7.3], was significantly higher than on day 7, 2.7 ng/mL [2.3, 3.2]. Analogously, L_{max} on day 14, 8008 μm [7358, 8710], was significantly higher than on day 7, 4303 μm [4051, 4567]. There were no significant differences for L_{min} when comparing day 7 and day 14. On day 14, bFGF concentrations of 5 ng/mL and higher yielded NHDF densities that were significantly greater than 0.1 ng/mL. Additionally, bFGF concentrations of 5 ng/mL and higher generated greater NHDF densities on day 14 versus day 7.

3.2 Morphology of the ARS and gel-in-gel construct

The size distribution of the PFHep emulsion, measured with a Coulter counter, is shown in Figure 4A. The emulsion had a mean diameter of 6.2 ± 0.13 μm and a coefficient of variance of 13.4% ±0.6%. As seen in Figure 4B, the morphology of the double emulsion and the ARS was confirmed using confocal microscopy. The droplets appear relatively uniform in size, with the W_1 phase appearing green due to the presence of Alexa Fluor 488-labeled dextran in the W_1 phase. The PFHep phase within each droplet appears dark due to its lack of fluorescence. Despite the higher density of the droplets relative to fibrin, given that the density of PFHep is 1.7 g/mL, droplets were distributed throughout the entire height (i.e., z-direction) of the ARS. This was likely due to the quick polymerization time of the ARS. The macrostructure of the fibrin hydrogel can also be seen due to the inclusion of Alexa Fluor 647-labeled fibrinogen.

Figure 1B displays macroscopic images of the gel-in-gel constructs on day 7. Constructs with ARSs (i.e., inner gel) that were not exposed to US lacked bubble formation, which indicated the absence of ADV. All constructs appeared bubble free on day 0, prior to US exposure. Bubble formation in the ARSs correlated with the US pressure and emulsion volume.

3.3 ADV, in the absence of bFGF delivery, impacted sprouting

The total tubule length for constructs cultured in fully supplemented media (4235 ± 1816 μm) was 16-fold higher compared to constructs cultured in starvation media (258 ± 77 μm) (Figure 5A). To account for any effect of ADV itself on sprouting, gel-in-gel constructs were fabricated containing blank (i.e., without bFGF) emulsion. As seen in Figure 5B, three out of four conditions yielded between 1.6-1.7-fold greater sprout formation than the starvation condition. Overall, however, tubule formation in the absence of bFGF delivery was lower than conditions in Figure 3A that yielded significant sprouting.

3.4 ADV enhanced bFGF release and sprout formation

Gel-in-gel constructs were fabricated with bFGF-loaded emulsion in the ARS, exposed to US, and cultured for 7 days. Figure 6 displays the quantified total tubule formation. Both -US conditions as well as the 3.3 MPa PRP exposure with 0.25% (v/v) emulsion yielded sprouting that was not different than the starvation condition in Figure 5A. Significantly greater sprouting was measured following exposure of the 1% (v/v) ARS at 3.3 MPa PRP, 0.25% (v/v) ARS at 8.8 MPa PRP, and 1% (v/v) ARS at 8.8 MPa PRP. Overall, sprouting correlated with the volume fraction of bFGF-loaded emulsion in the ARS and the acoustic pressure used for bFGF release. The largest amount of sprouting was observed with a 1% (v/v) ARS at 8.8 MPa PRP (3282 ± 953 μm), which was 22% lower than the fully supplemented condition in Figure 5A.

To assess the distribution of bFGF in our *in vitro* system, an analogous experiment was run using acellular gel-in-gel constructs. As seen in Figure 7A and 7B, the fraction of bFGF released into the overlying media increased significantly following US exposure at 3.3 MPa PRP or 8.8 MPa PRP. Negligible release (i.e., < 0.02%) was measured for the -US conditions. bFGF release correlated with acoustic pressure for each emulsion concentration.

In response to exposure at 8.8 MPa PRP, greater bFGF release was measured from the ARS containing 1% (v/v) bFGF-loaded emulsion versus 0.25% (v/v); no difference was observed with the 3.3 MPa PRP exposure.

We measured the release profile from constructs containing bFGF directly incorporated into the inner fibrin gel (Figure 7C). In this scenario, the inner gel did not contain any emulsion and the masses of bFGF incorporated were equivalent to the 0.25% (v/v) (i.e., 167 ng) and 1% (v/v) (i.e., 668 ng) ARS conditions. For both mass loadings, values of C_{max} and K were not statistically different. C_{max} was 23.5% [22.4, 24.7] and 22.1% [21.2, 23.1] for constructs with 167 ng and 668 ng of bFGF, respectively. K was 1.1 day^{-1} [0.8, 1.6] and 0.9 day^{-1} [0.7, 1.2] for constructs with 167 ng and 668 ng of bFGF, respectively.

Samples of the outer gel were biopsied and digested to determine the concentration of bFGF in the outer gel. This was done to assess the effective concentration of bFGF that the HUVECs and NHDFs were exposed to in the analogous cell-based experiment (Figure 6). The relative distributions of bFGF in the inner gel, outer gel, and media are shown in Figure 7D and Figure 7E for day 2 and day 8, respectively. The validity of this mass balance approach was confirmed by digesting samples of the inner gel for the constructs without emulsion. These validation studies yielded close to complete recovery of the bFGF added. As seen in Figure 7D and 7E, the majority of the added bFGF remained in the inner gel for all conditions. For each experimental condition, the fraction of the bFGF in the inner gel or media increased when comparing day 2 versus day 8. On day 2, the fraction of bFGF in the media was significantly higher, compared to the inner gel, for the following conditions: fibrin + 668 ng bFGF, 1% (v/v) ARS exposed to US at 3.3 MPa PRP, fibrin + 167 ng bFGF, and 0.25% (v/v) ARS exposed to US at 3.3 MPa PRP. Comparatively, on day 8, the following conditions yielded significantly higher fractions of bFGF in the media versus the outer gel: fibrin + 668 ng bFGF, 1% (v/v) ARS exposed to US at 8.8 MPa PRP, fibrin + 167 ng bFGF, and 0.25% (v/v) ARS exposed to US at 3.3 MPa PRP. The concentration of bFGF in the outer gel is shown in Supplemental Figure 1.

3.5 Temporal presentation of bFGF

The impact of temporally staggering the release of bFGF from the gel-in-gel constructs containing ARSs was investigated using the experimental design in Table 1. Release was staggered by exposing different subvolumes of the ARS (e.g., none, half, complete) to US on day 1. At a later timepoint, the other half of the ARS was exposed to US. As shown in Figure 8A, total tubule length increased with incubation time within a given group of conditions (i.e., C, D, E). All +US conditions yielded significantly greater sprouting than the -US groups. However, there were no observed differences in sprouting when comparing the different US exposure patterns with the same incubation period (i.e., C1 vs D1 vs E1; C2 vs D2; C3 vs E2). Similar trends were observed with NHDF density (Figure 8B).

3.6 Spatial dependence of sprouting

Given the spatial distribution of the HUVEC-coated microbeads in the outer gel, we assessed whether the length of sprouting was dependent on the distance between the microbead and the ARS (i.e., inner gel). An example map, showing the locations of the

microbeads relative to the inner gel, is displayed (Supplemental Figure 2A). For all conditions in Figure 6 and Figure 8, an analysis of total tubule length versus distance from the ARS revealed no correlation based on a slope analysis (i.e., the 95% confidence of the calculated slope included zero for all constructs). Supplemental Figure 2B shows an example plot.

4 Discussion

bFGF has been shown to induce endothelial cell migration [33, 34] and tubule formation [35], as well as stimulate proliferation of dermal fibroblasts [36]. By encapsulating bFGF within a sonosensitive emulsion, bFGF release and endothelial sprouting were non-invasively controlled using US. This on-demand modulation of bFGF release using an ARS could have applicability in the translation of therapies using pro-angiogenic GFs.

Angiogenic sprouting correlated with the volume of emulsion in the ARS as well as the US pressure used to generate ADV. The amount of bFGF loaded into an ARS was dependent on the concentration of bFGF in the W_1 phase, the relative ratio of W_1 to PFC phases, and the volume percent of emulsion in the ARS. Given that the first two parameters were held constant in these studies, an ARS with 1% (v/v) emulsion had a greater mass loading of bFGF than an ARS with 0.25% (v/v) emulsion. At 8.8 MPa PRP, a greater volume of the US focus was suprathreshold than at 3.3 MPa PRP. Thus, the efficiency of bFGF release increased as a larger fraction of the emulsion in the ARS was exposed to multiple suprathreshold pulses. The correlation between payload release and acoustic pressure was also shown previously for sonosensitive emulsions with PFHep [31].

In the absence of US exposure, the levels of bFGF release, endothelial sprouting, and gas bubble formation were minimal. The PFC phase within the double emulsion, which surrounded the W_1 droplets, acted as a diffusion barrier for bFGF since PFCs are extremely hydrophobic [37]. Thus, payload release correlated with the disruption of the PFC layer within the emulsion, which was selectively controlled by ADV and the application of US. For lower boiling point PFCs, thermal destabilization can generate non-specific payload release and bubble formation in the absence of suprathreshold US [22, 38]. In the current study, PFHep, which has a bulk boiling point of 83°C, was used as the PFC phase. Therefore, not even considering any boiling point elevation due to the Laplace pressure within the droplets [39, 40], the boiling of PFHep greatly exceeded the environmental temperature of the gel-in-gel constructs (i.e., 37°C).

As observed macroscopically, following ADV, an irreversible expansion and deformation of the fibrin matrix occurred in the ARS. This bubble induced deformation can consolidate the fibrin surrounding the bubbles, increase the bulk stiffness of the ARS, and increase the rate of fibrin degradation [17, 41]. There are two hypotheses regarding the composition of these bubbles, which were generated by ADV. First, ADV generated stable bubbles of PFHep in the ARS, which could subsequently in-gas and expand [19]. However, given the high boiling point of PFHep, this scenario seemed unlikely since the PFHep vapor would have been supercooled. Second, ADV caused transient vaporization of the PFHep [42], which lead to release of bFGF and recondensation of the liquid PFC. The liquid PFHep remained

undissolved in the ARS, due the low aqueous solubility of PFHep (i.e., 0.01 mg/L [43]). In this scenario, the recondensation of PFHep is likely only if the bubble non-inertially collapses [44]. In both scenarios, the high solubility of oxygen in PFHep (i.e., 55% (v/v) versus 3% (v/v) in water [45]) could have facilitated the nucleation event for ADV [46] and the growth of the bubbles within the ARS.

The presence of bubbles within the ARS impacted the rate of bFGF release. When directly incorporated into fibrin, a burst release of bFGF occurs [47], with the majority of bFGF retained in the matrix because of its ability to bind to heparin-binding domains of fibrin [48]. With an ARS, the presence of the bubbles slowed the rate at which bFGF diffused into the overlying media and outer gel. Given that bFGF cannot diffuse through a bubble, but rather must go around it, the effective path length for diffusion in an ARS with bubbles was therefore longer. When comparing bFGF release into the media following exposure at 8.8 MPa PRP, the rate of release qualitatively correlated inversely with the volume fraction of emulsion in the ARS, which supports the hypothesis regarding an increased path length.

In the absence of bFGF delivery, the presence of the emulsion and bubbles within the ARS had a small, but statistically significant impact on angiogenic sprouting. We also previously observed this effect *in vivo* with subcutaneously-implanted ARSs [17]. One potential explanation is that the emulsion, and ADV of the emulsion [49], could cause a localized decrease in the oxygen concentration. When cultured in the absence of GFs, HUVECs form tube-like structures under hypoxic, but not normoxic, conditions; this was attributed to the hypoxia-inducible factor 1α-bFGF amplification pathway [50]. Thus, there could be a synergistic effect of delivering bFGF and modulating the local oxygen concentration for the observed sprouting.

Temporally staggering the release of bFGF from the ARS did not have an impact on angiogenic sprouting. In another *in vitro* study, early exposure to a high concentration of pro-angiogenic GFs yielded the greatest amount of endothelial sprouting relative to other dosing schemes [51]. As seen in Supplemental Figure 1, the bFGF concentration in the outer gel was 3.0 ng/mL on day 2 and 9.2 ng/mL on day 8, following ADV in the entire ARS, containing 1% (v/v) emulsion, at 8.8 MPa PRP (i.e., similar to groups C1-C3). For groups D and E, where only half of the ARS was initially exposed to US, the bFGF concentrations in the outer gel would be half. As seen in the bFGF dose response data (Figure 3A), there was no difference in sprouting at bFGF concentrations of 2 ng/mL to 5 ng/mL when comparing day 7 and day 14. Therefore, it is hypothesized that the concentration of released bFGF may not have been high enough to observe a difference in sprouting using the different temporal patterns of bFGF release.

Tubule length was not dependent on the distance between each HUVEC-coated microbead and the ARS (Supplemental Figure 2). The diffusivity of bFGF at 37°C in water, estimated using the Stokes-Einstein equation, is 2.2×10^{-6} cm^2/s [52]. The measured effective diffusivities of varying molecular weight dextrans in fibrin matrices have shown good agreement with values predicted by the Stokes-Einstein equation [23]. As a first-order, one-dimensional approximation, the time required for bFGF to diffuse from the center of the inner gel to the periphery of the outer gel or periphery of the inner gel to the periphery of the

outer gel would be 4 days or 1.7 days, respectively. Thus, any spatial gradient of bFGF generated by ADV would ultimately be unstable due to diffusion over the course of the experiment.

A potential limitation of the current study is that the HUVEC-coated microbeads and NHDFs were spatially separated from the ARS. As such, the effect of US exposure and ADV on tubule formation was not elucidated. For this study, to assist with imaging and quantifying tubule formation, the cells were not included in the ARS since the presence of bubbles impede optical microscopy of intact constructs. In our previous studies, the metabolic activity of HUVECs or C3H/10T1/2 cells, encapsulated within ARSs was not negatively impacted by the ADV [41]. In another study, the viability of C3H/10T1/2 cells decreased slightly with increasing US pressure used to generate ADV within the ARS [38]. In our previous in vivo experiments [17, 18], we did not note any US-induced damage to tissues surrounding the implanted ARSs following exposure to US at similar acoustic pressures used in the current study.

5 Conclusions

The study demonstrates that non-invasive, focused US can enhance endothelial network formation in a co-culture model of angiogenic sprouting via the controlled release of bFGF. A gel-in-gel construct was used to evaluate the impact of US-controlled delivery, whereby the center gel contained bFGF encapsulated within a monodispersed, sonosensitive emulsion. In the absence of ADV, release of bFGF from the ARS was minimal whereas in response to suprathreshold US, bFGF release correlated with acoustic pressure. The length of sprouting correlated with the volume of bFGF-loaded emulsion in the ARS and the acoustic pressure used for ADV. There was no correlation between tubule length and the distance between a HUVEC-coated microbead and the ARS. There was a small, but statistically significant enhancement of sprouting with blank emulsion and ADV. Staggering the release of bFGF did not impact total tubule lengths. Future studies will use ARSs to evaluate the impact of other pro-angiogenic molecules on endothelial sprouting and the *in vivo* translation of ARSs for therapeutic angiogenesis.

Supplementary Material

Refer to Web version on PubMed Central for supplementary material.

Acknowledgements

This work was supported by NIH Grant R01HL139656 (M.L.F.). X.D. was supported by the National Key R&D Program of China 2017YFC0107300 and the China Scholarship Council. Special thanks to Dr. Allen Brooks for assisting with the synthesis of the fluorosurfactant.

REFERENCES

[1]. Deveza L, Choi J, Yang F, Therapeutic Angiogenesis for Treating Cardiovascular Diseases, Theranostics 2(8) (2012) 801–814. [PubMed: 22916079]

[2]. Hughes GC, Biswas SS, Yin BL, Coleman RE, DeGrado TR, Landolfo CK, Lowe JE, Annex BH, Landolfo KP, Therapeutic angiogenesis in chronically ischemic porcine myocardium:

Comparative effects of bFGF and VEGF, Ann Thorac Surg 77(3) (2004) 812–818. [PubMed: 14992878]

[3]. Takehara N, Tsutsumi Y, Tateishi K, Ogata T, Tanaka H, Ueyama T, Takahashi T, Takamatsu T, Fukushima M, Komeda M, Yamagishi M, Yaku H, Tabata Y, Matsubara H, Oh H, Controlled Delivery of Basic Fibroblast Growth Factor Promotes Human Cardiosphere-Derived Cell Engraftment to Enhance Cardiac Repair for Chronic Myocardial Infarction, Journal of the American College of Cardiology 52(23) (2008) 1858–1865. [PubMed: 19038683]

[4]. Hosaka A, Koyama H, Kushibiki T, Tabata Y, Nishiyama N, Miyata T, Shigematsu H, Takato T, Nagawa H, Gelatin hydrogel microspheres enable pinpoint delivery of basic fibroblast growth factor for the development of functional collateral vessels, Circulation 110(21) (2004) 3322–3328. [PubMed: 15520306]

[5]. Horio T, Fujita M, Tanaka Y, Ishihara M, Kishimoto S, Nakamura S, Hase K, Maehara T, Efficacy of fragmin/protamine microparticles containing fibroblast growth factor-2 (F/P MPs/FGF-2) to induce collateral vessels in a rabbit model of hindlimb ischemia, Journal of vascular surgery 54(3) (2011) 791–798. [PubMed: 21620612]

[6]. Simons M, Annex BH, Laham RJ, Kleiman N, Henry T, Dauerman H, Udelson JE, Gervino EV, Pike M, Whitehouse MJ, Moon T, Chronos NA, Pharmacological treatment of coronary artery disease with recombinant fibroblast growth factor-2: double-blind, randomized, controlled clinical trial, Circulation 105(7) (2002) 788–93. [PubMed: 11854116]

[7]. Laham RJ, Sellke FW, Edelman ER, Pearlman JD, Ware JA, Brown DL, Gold JP, Simons M, Local perivascular delivery of basic fibroblast growth factor in patients undergoing coronary bypass surgery - Results of a phase I randomized, double-blind, placebo-controlled trial, Circulation 100(18) (1999) 1865–1871. [PubMed: 10545430]

[8]. Lederman RJ, Mendelsohn FO, Anderson RD, Saucedo JF, Tenaglia AN, Hermiller JB, Hillegass WB, Rocha-Singh K, Moon TE, Whitehouse MJ, Annex BH, Investigators T, Therapeutic angiogenesis with recombinant fibroblast growth factor-2 for intermittent claudication (the TRAFFIC study): a randomised trial, Lancet 359(9323) (2002) 2053–8. [PubMed: 12086757]

[9]. Marui A, Tabata Y, Kojima S, Yamamoto M, Tambara K, Nishina T, Saji Y, Inui K, Hashida T, Yokoyama S, Onodera R, Ikeda T, Fukushima M, Komeda M, A novel approach to therapeutic angiogenesis for patients with critical limb ischemia by sustained release of basic fibroblast growth factor using biodegradable gelatin hydrogel: an initial report of the phase I-IIa study, Circ J 71(8) (2007) 1181–6. [PubMed: 17652878]

[10]. Hashimoto T, Koyama H, Miyata T, Hosaka A, Tabata Y, Takato T, Nagawa H, Selective and Sustained Delivery of Basic Fibroblast Growth Factor (bFGF) for Treatment of Peripheral Arterial Disease: Results of a Phase I Trial, Eur J Vasc Endovasc 38(1) (2009) 71–75.

[11]. Kumagai M, Marui A, Tabata Y, Takeda T, Yamamoto M, Yonezawa A, Tanaka S, Yanagi S, Ito-Ihara T, Ikeda T, Murayama T, Teramukai S, Katsura T, Matsubara K, Kawakami K, Yokode M, Shimizu A, Sakata R, Safety and efficacy of sustained release of basic fibroblast growth factor using gelatin hydrogel in patients with critical limb ischemia, Heart Vessels 31(5) (2016) 713–721. [PubMed: 25861983]

[12]. Silva AKA, Richard C, Bessodes M, Scherman D, Merten OW, Growth Factor Delivery Approaches in Hydrogels, Biomacromolecules 10(1) (2009) 9–18. [PubMed: 19032110]

[13]. Wang ZM, Wang ZF, Lu WW, Zhen WX, Yang DZ, Peng SL, Novel biomaterial strategies for controlled growth factor delivery for biomedical applications, Npg Asia Mater 9 (2017).

[14]. Yang HS, Bhang SH, Hwang JW, Kim DI, Kim BS, Delivery of Basic Fibroblast Growth Factor Using Heparin-Conjugated Fibrin for Therapeutic Angiogenesis, Tissue Eng Pt A 16(6) (2010) 2113–2119.

[15]. Jeon O, Kang SW, Lim HW, Chung JH, Kim BS, Long-term and zero-order release of basic fibroblast growth factor from heparin-conjugated poly(L-lactide-co-glycolide) nanospheres and fibrin gel, Biomaterials 27(8) (2006) 1598–1607. [PubMed: 16146647]

[16]. Guo XL, Elliott CG, Li ZQ, Xu YY, Hamilton DW, Guan JJ, Creating 3D Angiogenic Growth Factor Gradients in Fibrous Constructs to Guide Fast Angiogenesis, Biomacromolecules 13(10) (2012) 3262–3271. [PubMed: 22924876]

[17]. Moncion A, Arlotta KJ, O'Neill EG, Lin M, Mohr LA, Franceschi RT, Kripfgans OD, Putnam AJ, Fabiilli ML, In vitro and in vivo assessment of controlled release and degradation of acoustically-responsive scaffolds, Acta Biomater 46 (2016) 221–33. [PubMed: 27686040]

[18]. Moncion A, Lin M, O'Neill EG, Franceschi RT, Kripfgans OD, Putnam AJ, Fabiilli ML, Controlled release of basic fibroblast growth factor for angiogenesis using acoustically-responsive scaffolds, Biomaterials 140 (2017) 26–36. [PubMed: 28624705]

[19]. Kripfgans OD, Fowlkes JB, Miller DL, Eldevik OP, Carson PL, Acoustic droplet vaporization for therapeutic and diagnostic applications, Ultrasound Med Biol 26(7) (2000) 1177–1189. [PubMed: 11053753]

[20]. Li DS, Kripfgans OD, Fabiilli ML, Brian Fowlkes J, Bull JL, Initial nucleation site formation due to acoustic droplet vaporization, Applied physics letters 104(6) (2014) 063703. [PubMed: 24711671]

[21]. Shpak O, Verweij M, Vos HJ, de Jong N, Lohse D, Versluis M, Acoustic droplet vaporization is initiated by superharmonic focusing, Proceedings of the National Academy of Sciences of the United States of America 111(5) (2014) 1697–702. [PubMed: 24449879]

[22]. Moncion A, Lin M, Kripfgans OD, Franceschi RT, Putnam AJ, Fabiilli ML, Sequential payload release from acoustically-responsive scaffolds uinsg focused ultrasound, Ultrasound Med Biol 44(11) (2018) 2323–2335. [PubMed: 30077413]

[23]. Ghajar CM, Chen X, Harris JW, Suresh V, Hughes CCW, Jeon NL, Putnam AJ, George SC, The effect of matrix density on the regulation of 3-D capillary morphogenesis, Biophys J 94(5) (2008) 1930–1941. [PubMed: 17993494]

[24]. Juliar BA, Keating MT, Kong YP, Botvinick EL, Putnam AJ, Sprouting angiogenesis induces significant mechanical heterogeneities and ECM stiffening across length scales in fibrin hydrogels, Biomaterials 162 (2018) 99–108. [PubMed: 29438884]

[25]. Nakatsu MN, Sainson RCA, Aoto JN, Taylor KL, Aitkenhead M, Perez-del-Pulgar S, Carpenter PM, Hughes CCW, Angiogenic sprouting and capillary lumen formation modeled by human umbilical vein endothelial cells (HUVEC) in fibrin gels: the role of fibroblasts and Angiopoietin-1, Microvasc Res 66(2) (2003) 102–112. [PubMed: 12935768]

[26]. Ghajar CM, Kachgal S, Kniazeva E, Mori H, Costes SV, George SC, Putnam AJ, Mesenchymal cells stimulate capillary morphogenesis via distinct proteolytic mechanisms, Experimental cell research 316(5) (2010) 813–25. [PubMed: 20067788]

[27]. Anderson EM, Mooney DJ, The Combination of Vascular Endothelial Growth Factor and Stromal Cell-Derived Factor Induces Superior Angiogenic Sprouting by Outgrowth Endothelial Cells, Journal of vascular research 52(1) (2015) 62–69. [PubMed: 26045306]

[28]. Sommer A, Rifkin DB, Interaction of Heparin with Human Basic Fibroblast Growth-Factor - Protection of the Angiogenic Protein from Proteolytic Degradation by a Glycosaminoglycan, J Cell Physiol 138(1) (1989) 215–220. [PubMed: 2910884]

[29]. Griffith CK, Miller C, Sainson RCA, Calvert JW, Jeon NL, Hughes CCW, George SC, Diffusion limits of an in vitro thick prevascularized tissue, Tissue engineering 11(1-2) (2005) 257–266. [PubMed: 15738680]

[30]. Nehls V, Drenckhahn D, A Novel, Microcarrier-Based in-Vitro Assay for Rapid and Reliable Quantification of 3-Dimensional Cell-Migration and Angiogenesis, Microvasc Res 50(3) (1995) 311–322. [PubMed: 8583947]

[31]. Lu X, Dong X, Natla S, Kripfgans OD, Fowlkes JB, Wang X, Franceschi RT, Putnam AJ, Fabiilli ML, Parametric study of acoustic droplet vaporization thresholds and payload release from acoustically-responsive scaffolds, Ultrasound Med Biol under review (2019).

[32]. Li SR, Nih LR, Bachman H, Fei P, Li YL, Nam E, Dimatteo R, Carmichael ST, Barker TH, Segura T, Hydrogels with precisely controlled integrin activation dictate vascular patterning and permeability, Nature materials 16(9) (2017) 953-+. [PubMed: 28783156]

[33]. Vernon RB, Sage EH, A novel, quantitative model for study of endothelial cell migration and sprout formation within three-dimensional collagen matrices, Microvasc Res 57(2) (1999) 118–133. [PubMed: 10049660]

[34]. Nehls V, Herrmann R, Huhnken M, Guided migration as a novel mechanism of capillary network remodeling is regulated by basic fibroblast growth factor, Histochem Cell Biol 109(4) (1998) 319–329. [PubMed: 9562381]

[35]. Chabut D, Fischer AM, Colliec-Jouault S, Laurendeau I, Matou S, Le Bonniec B, Helley D, Low molecular weight fucoidan and heparin enhance the basic fibroblast growth factor-induced tube formation of endothelial cells through heparan sulfate-dependent alpha6 overexpression, Mol Pharmacol 64(3) (2003) 696–702. [PubMed: 12920206]

[36]. de la Puente P, Ludena D, Fernandez A, Aranda JL, Varela G, Iglesias J, Autologous fibrin scaffolds cultured dermal fibroblasts and enriched with encapsulated bFGF for tissue engineering, Journal of Biomedical Materials Research Part A 99a(4) (2011) 648–654.

[37]. Riess JG, Understanding the fundamentals of perfluorocarbons and perfluorocarbon emulsions relevant to in vivo oxygen delivery, Artif Cell Blood Sub 33(1) (2005) 47–63.

[38]. Moncion A, Arlotta KJ, Kripfgans OD, Fowlkes JB, Carson PL, Putnam AJ, Franceschi RT, Fabiilli ML, Design and Characterization of Fibrin-Based Acoustically Responsive Scaffolds for Tissue Engineering Applications, Ultrasound Med Biol 42(1) (2016) 257–71. [PubMed: 26526782]

[39]. Rapoport NY, Kennedy AM, Shea JE, Scaife CL, Nam K-H, Controlled and targeted tumor chemotherapy by ultrasound-activated nanoemulsions/microbubbles, Journal of Controlled Release 138(2) (2009) 268–276. [PubMed: 19477208]

[40]. Sheeran PS, Luois S, Dayton PA, Matsunaga TO, Formulation and Acoustic Studies of a New Phase-Shift Agent for Diagnostic and Therapeutic Ultrasound, Langmuir 27(17) (2011) 10412–10420. [PubMed: 21744860]

[41]. Fabiilli ML, Wilson CG, Padilla F, Martin-Saavedra FM, Fowlkes JB, Franceschi RT, Acoustic droplet-hydrogel composites for spatial and temporal control of growth factor delivery and scaffold stiffness, Acta Biomater 9(7) (2013) 7399–409. [PubMed: 23535233]

[42]. Reznik N, Shpak O, Gelderblom EC, Williams R, de Jong N, Versluis M, Burns PN, The efficiency and stability of bubble formation by acoustic vaporization of submicron perfluorocarbon droplets, Ultrasonics 53(7) (2013) 1368–1376. [PubMed: 23652262]

[43]. Kabalnov AS, Makarov KN, Shcherbakova OV, Solubility of Fluorocarbons in Water as a Key Parameter Determining Fluorocarbon Emulsion Stability, J Fluorine Chem 50(3) (1990) 271–284.

[44]. Matula TJ, Hilmo PR, Storey BD, Szeri AJ, Radial response of individual bubbles subjected to shock wave lithotripsy pulses in vitro, Phys Fluids 14(3) (2002) 913–921.

[45]. Riess JG, Oxygen Carriers ("Blood Substitutes") - Raison d'Etre, Chemistry, and Some Physiology, Chemical Reviews 101(9) (2001) 2797–2919. [PubMed: 11749396]

[46]. Rapoport N, Nam KH, Gupta R, Gao Z, Mohan P, Payne A, Todd N, Liu X, Kim T, Shea J, Scaife C, Parker DL, Jeong EK, Kennedy AM, Ultrasound-mediated tumor imaging and nanotherapy using drug loaded, block copolymer stabilized perfluorocarbon nanoemulsions, Journal of controlled release : official journal of the Controlled Release Society 153(1) (2011) 4–15. [PubMed: 21277919]

[47]. Jeon O, Ryu SH, Chung JH, Kim BS, Control of basic fibroblast growth factor release from fibrin gel with heparin and concentrations of fibrinogen and thrombin, Journal of Controlled Release 105(3) (2005) 249–259. [PubMed: 16088988]

[48]. Martino MM, Briquez PS, Ranga A, Lutolf MP, Hubbell JA, Heparin-binding domain of fibrin(ogen) binds growth factors and promotes tissue repair when incorporated within a synthetic matrix, Proceedings of the National Academy of Sciences of the United States of America 110(12) (2013) 4563–4568. [PubMed: 23487783]

[49]. Radhakrishnan K, Holland CK, Haworth KJ, Scavenging dissolved oxygen via acoustic droplet vaporization, Ultrasonics sonochemistry 31 (2016) 394–403. [PubMed: 26964964]

[50]. Calvani M, Rapisarda A, Uranchimeg B, Shoemaker RH, Melillo G, Hypoxic induction of an HIF-1 alpha-dependent bFGF autocrine loop drives angiogenesis in human endothelial cells, Blood 107(7) (2006) 2705–2712. [PubMed: 16304044]

[51]. Brudno Y, Ennett-Shepard AB, Chen RR, Aizenberg M, Mooney DJ, Enhancing microvascular formation and vessel maturation through temporal control over multiple pro-angiogenic and pro-maturation factors, Biomaterials 34(36) (2013) 9201–9209. [PubMed: 23972477]

[52]. Filion RJ, Popel AS, A reaction-diffusion model of basic fibroblast growth factor interactions with cell surface receptors, Annals of biomedical engineering 32(5) (2004) 645–663. [PubMed: 15171620]

Statement of Significance

Due to the ineffectiveness of conventional routes of administration, implantable hydrogels are often used as matrices to deliver growth factors (GFs). Spatial control of release is typically realized using anisotropic constructs while temporal control is obtained by modifying matrix properties and GF-scaffold interactions. In this study, we demonstrate how focused ultrasound can be used to non-invasively and spatiotemporally control release of basic fibroblast growth factor (bFGF), in an on-demand manner, from a composite hydrogel. The acoustically-responsive scaffold (ARS) consists of a bFGF-loaded, monodispersed double emulsion embedded within a fibrin matrix. We demonstrate how controlled release of bFGF can stimulate endothelial network formation. These results may be of interest to groups working on controlled release strategies for GFs, especially in the context of stimulating angiogenesis.

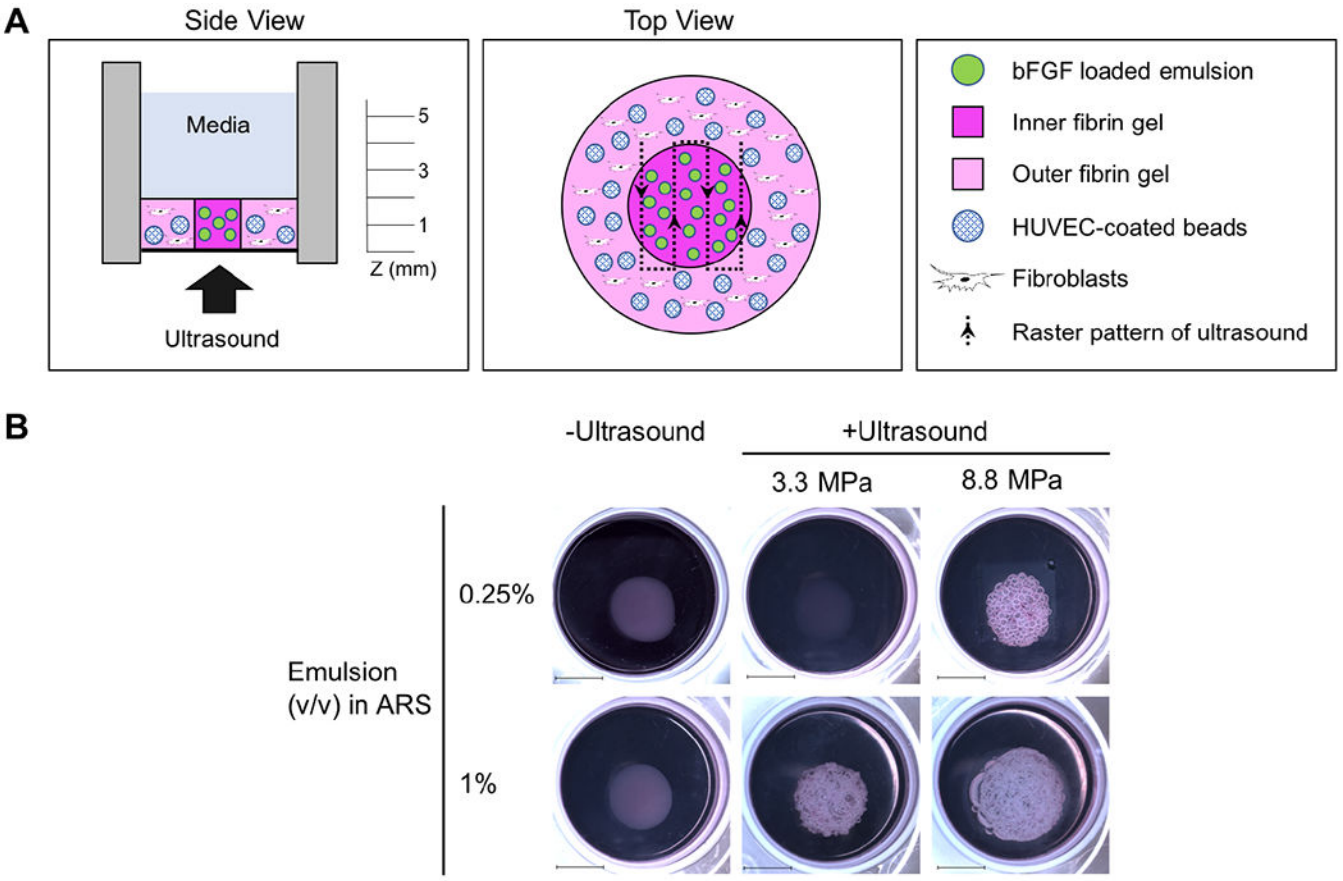

Figure 1.

A gel-in-gel construct was used to evaluate endothelial sprouting in response to the US-triggered delivery of bFGF. A) The inner fibrin gel contained a bFGF-loaded emulsion and was termed an acoustically-responsive scaffold (ARS). The outer fibrin gel contained HUVEC-coated microbeads and normal human dermal fibroblasts. The focus of the US transducer was rastered across the ARS to trigger release of the bFGF. B) Macroscopic images qualitatively display the morphologies of the constructs 7 days after US exposure. Macroscopic bubble formation was observed in ARSs with 0.25% (v/v) emulsion and exposed to 8.8 MPa PRP as well as in ARSs with 1% (v/v) and exposed to 3.3 MPa PRP or 8.8 MPa PRP. No obvious bubble formation was observed in the absence of US exposure. Scale bar: 1 cm.

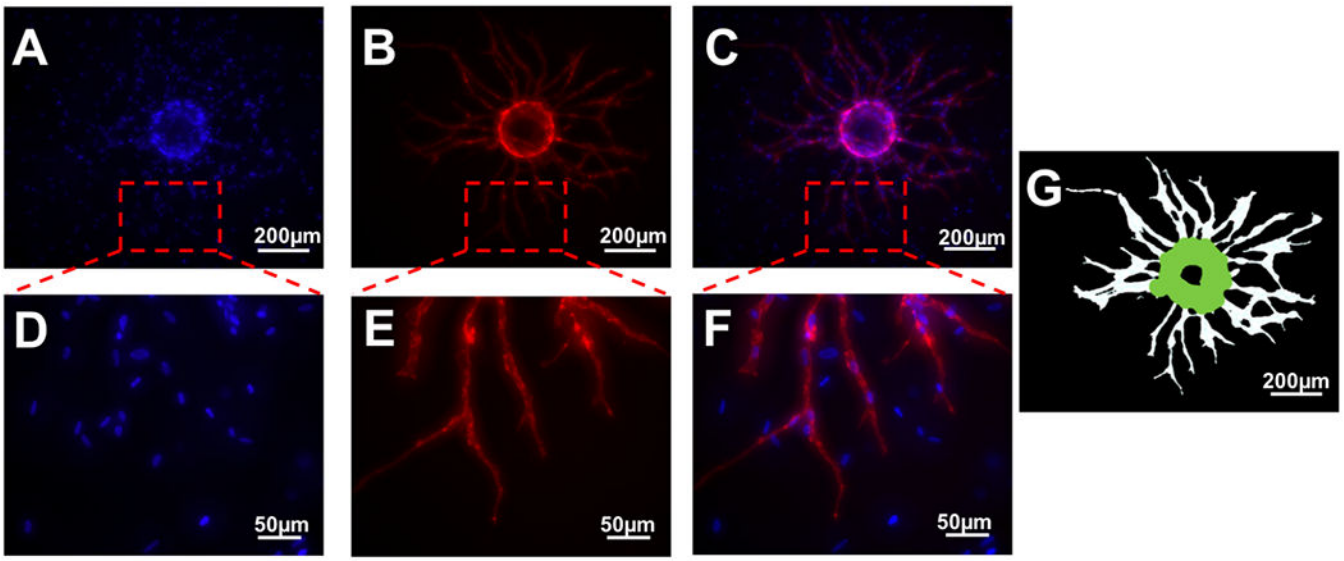

Figure 2.

Representative images of angiogenic sprouting at day 7. DAPI (A) and UEA-I (B) staining indicate total cell nuclei and HUVECs, respectively. A merged image is also shown (C). The bottom row (D-F) shows zoomed-in panels from the top row (A-C). Total tubule length was determined via software that thresholded and segmented the UEA-I stained images (G). Scale bars: 200 μm (top row) and 50 μm (bottom row), respectively.

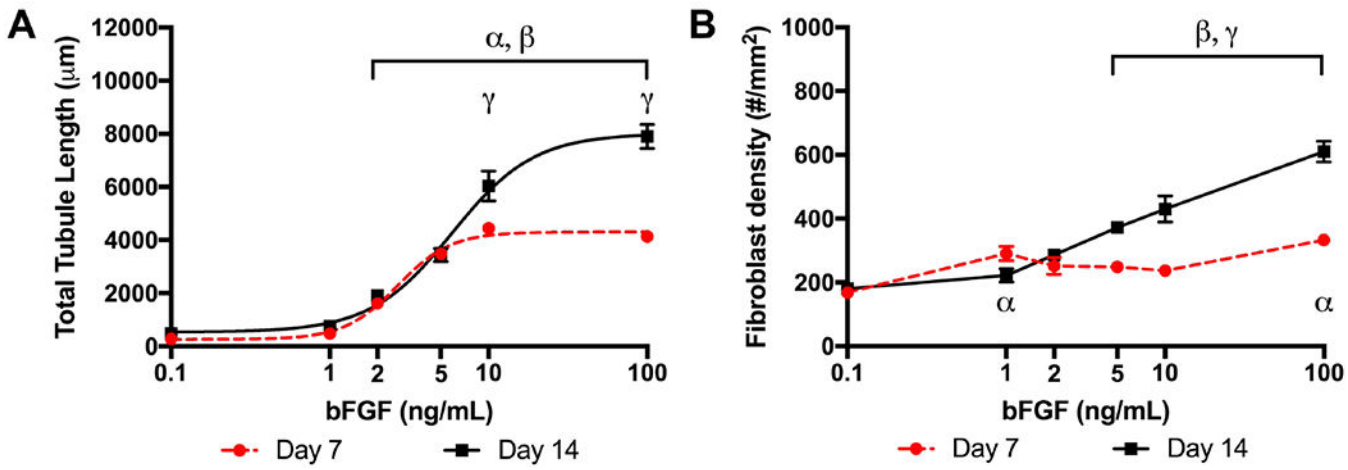

Figure 3.

Total tubule length and fibroblast density correlated with the bFGF concentration in the overlying media. (A) HUVECs were coated onto microcarrier beads and co-cultured with NHDFs for either 7 or 14 days in 2.5 mg/mL fibrin gels. Tubule formation displayed a sigmoidal response with bFGF concentration (7 beads assessed per replicate, N=3 per condition). (B) The density of NHDFs tended to increase with bFGF concentration (10 views assessed per replicate, N=3 per condition). Data are represented as mean ± standard error of the mean. Statistically significant differences are denoted as follows: α: vs 0.1 ng/mL on day 7, β: vs 0.1 ng/mL on day 14, and γ: day 7 vs day 14 for a fixed bFGF concentration.

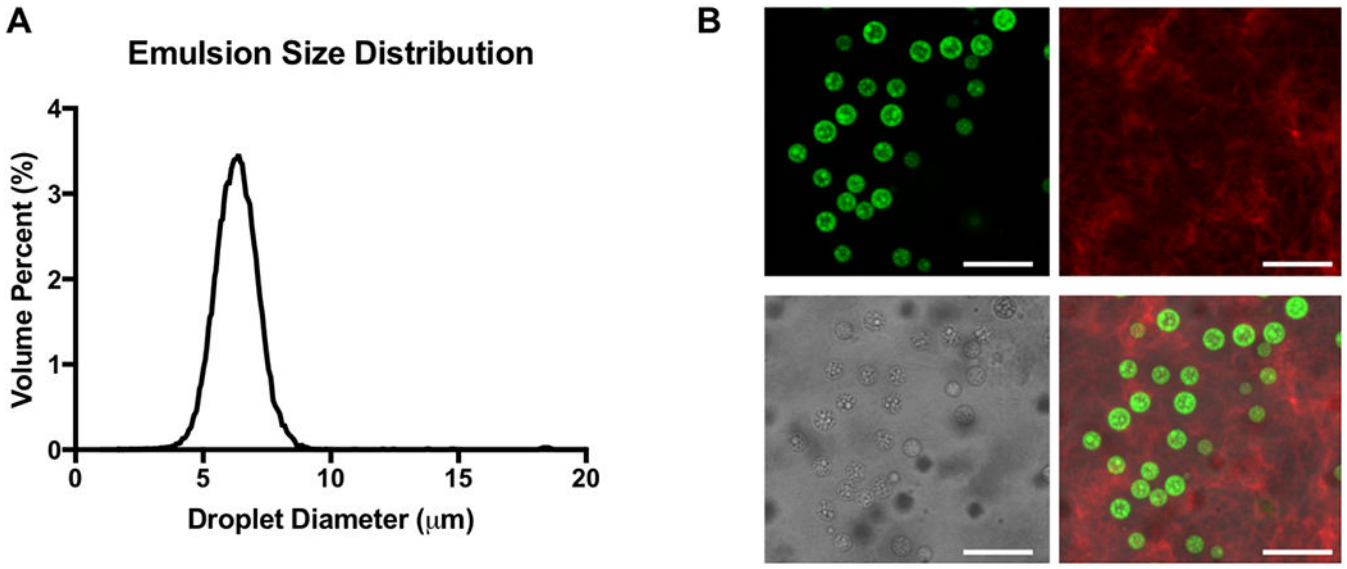

Figure 4.

bFGF was loaded into the W_1 phase of a monodisperse double emulsion. (A) Volume-weighted size distribution of the emulsion, which was generated using a two-step approach. The primary emulsion was made via sonication and then encapsulated in a microfluidic chip to produce the double emulsion. The mean diameter and coefficient of variance of the double emulsion were 6.2 ± 0.13 μm and 13.4% ± 0.6%, respectively. (B) Confocal microscopy images of an acoustically-responsive scaffold (ARS) containing a double emulsion with Alexa Fluor 488-labeled dextran in the W_1 phase (shown in green) at 100× magnification (top left). The ARS contained Alexa Fluor 647-labeled fibrinogen (top right). A brightfield image of the ARS shows the double emulsion (bottom left). Merged fluorescent image of the double emulsion and fibrinogen (bottom right). Scale bar: 20 μm.

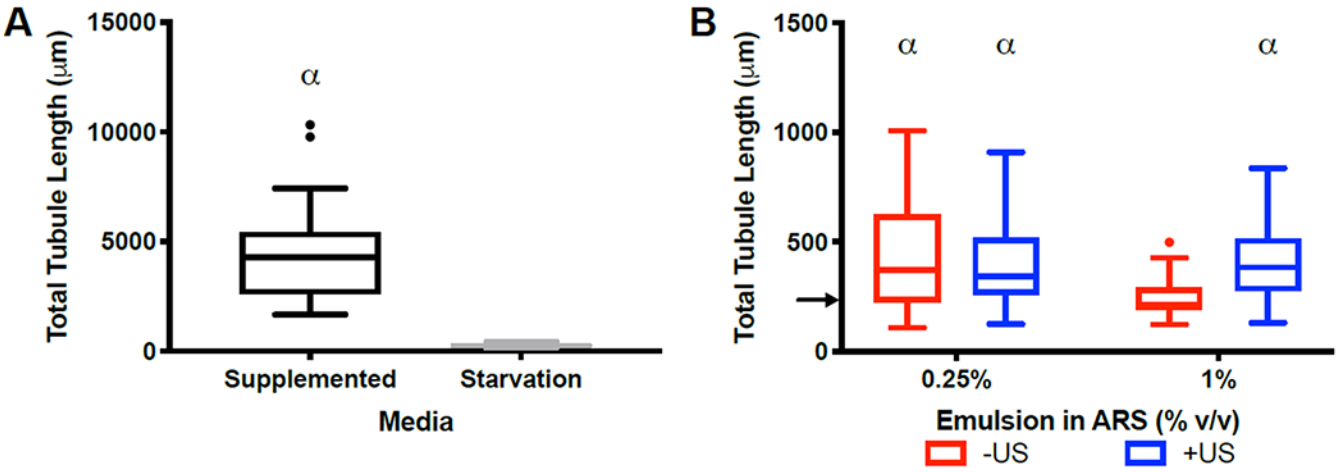

Figure 5.

Robust sprouting was observed in gel-in-gel constructs cultured in fully supplemented media, while a slight increase was seen with blank ARS constructs. (A) Significantly greater sprouting was obtained in constructs cultured in fully supplemented media versus starvation media at day 7 (20 beads assessed per replicate, N=4 per condition). The inner gel for both conditions was 2.5 mg/mL fibrin (i.e., without emulsion or cells). The outer gel contained HUVEC-coated microbeads and NHDFs (B) The impact of ADV on sprouting was investigated by fabricating gel-in-gel constructs with blank (i.e., without bFGF) emulsion in the center gel. The ARSs were exposed to US (2.5 MHz, 8.8 MPa PRP) on day 0. Three out of four conditions yielded greater sprouting than the starvation condition (12 beads assessed per replicate, N=4 per condition). Each boxed region displays the median and interquartile range (IQR) of the data. Whiskers show the range within 1.5 IQR. Statistically significant differences are denoted as follows: α: vs starvation condition. The arrow in Figure 5B denotes the median of the starvation control group from Figure 5A.

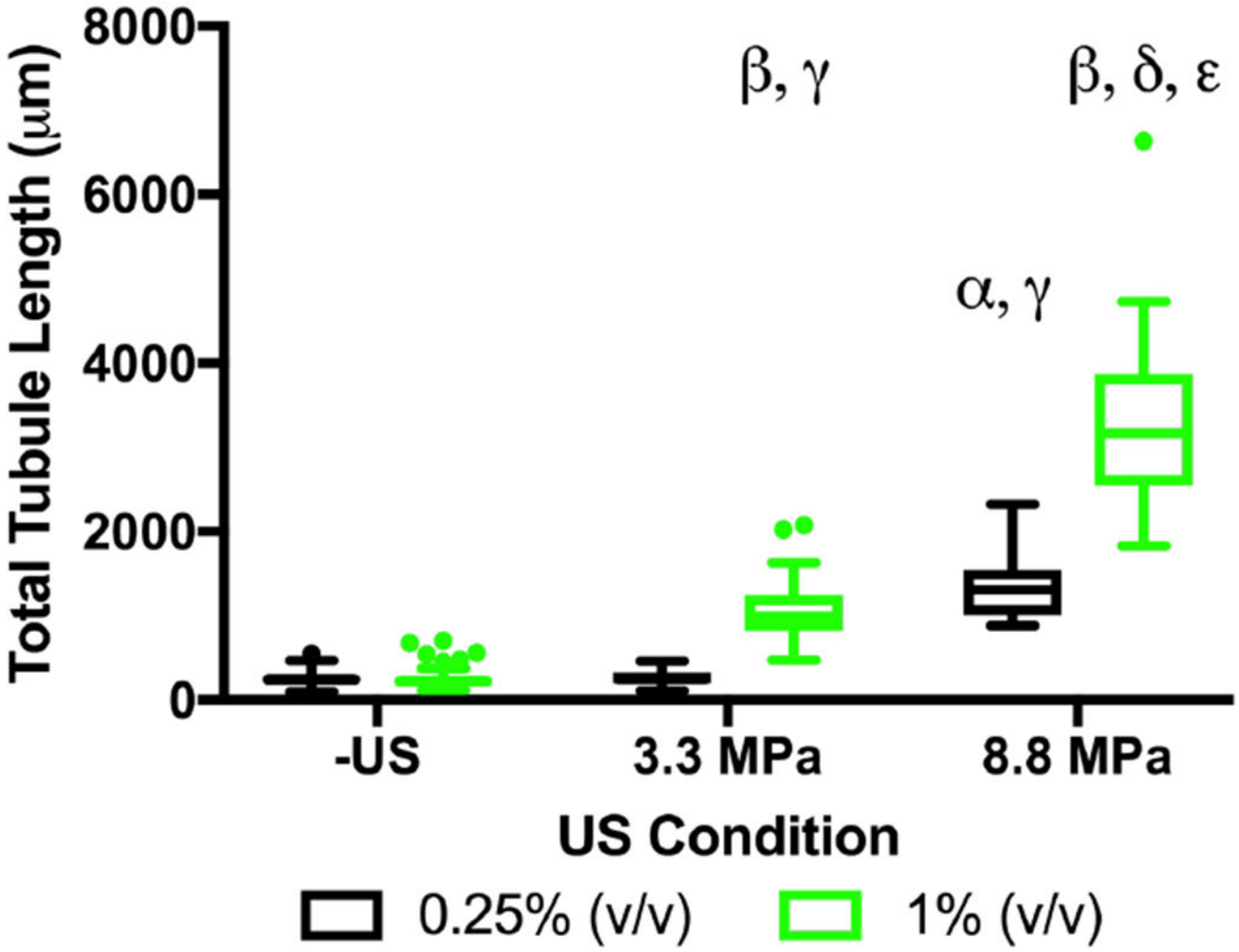

Figure 6.

Sprouting correlated with the volume fraction of the bFGF-loaded emulsion and acoustic pressure used for bFGF release. Gel-in-gel constructs were fabricated with ARSs, containing 0.25% or 1% (v/v) bFGF-loaded emulsion, as the inner gels. The outer gels contained HUVEC-coated microbeads and NHDFs. The ARSs were exposed to 2.5 MHz US on day 1. Total tubule length was measured at day 7 (10 beads assessed per replicate, N=4 per condition). Each boxed region displays the median and interquartile range (IQR) of the data. Whiskers show the range within 1.5 IQR. Statistically significant differences are denoted as follows: α: vs 0.25% (-US), β: vs 1% (-US), γ: vs 0.25% (3.3 MPa PRP), δ: 0.25% (8.8 MPa PRP), and ε: 1% (3.3 MPa PRP).

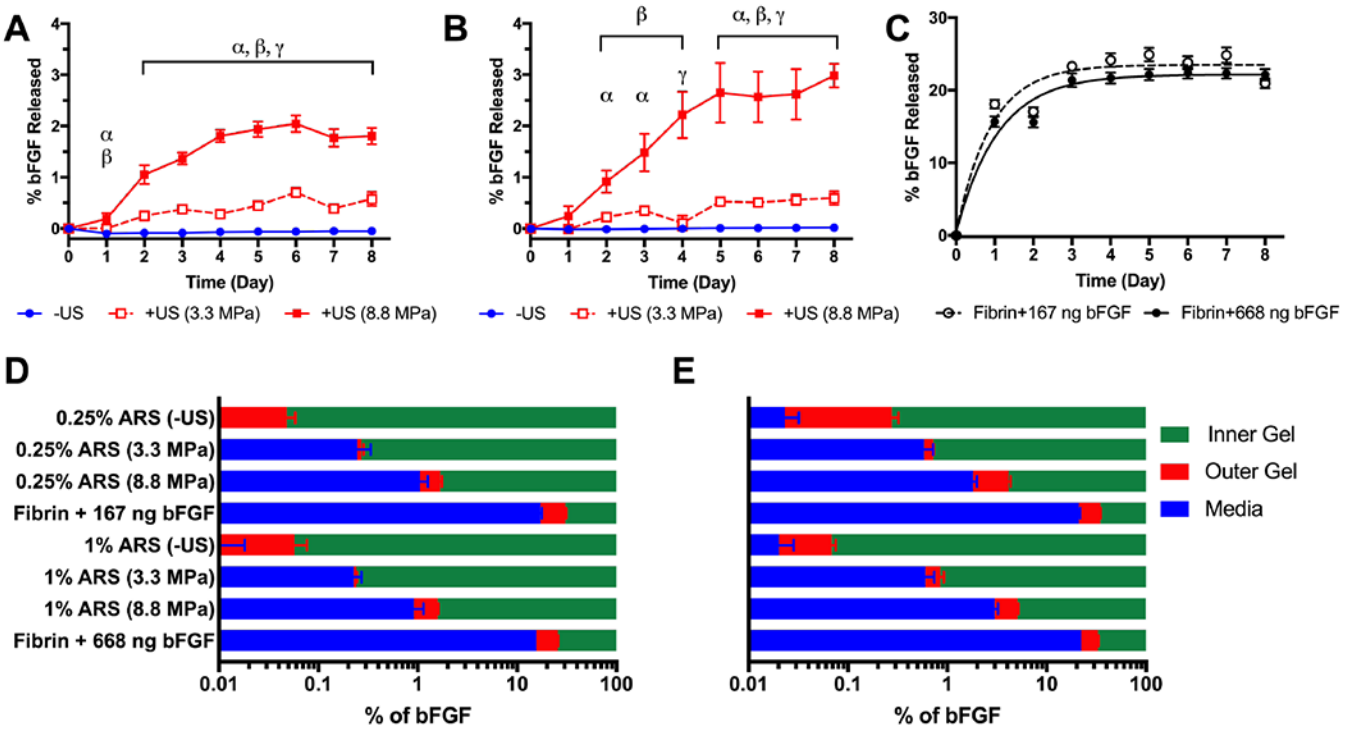

Figure 7.

bFGF released from the ARS was dependent on the emulsion volume as well as acoustic pressure of US. Gel-in-gel constructs were fabricated with ARSs, containing 0.25% or 1% (v/v) bFGF-loaded emulsion, as the inner gels. The outer gels contained 2.5 mg/mL fibrin without emulsion or cells. The ARSs were exposed to 2.5 MHz US on day 1. The amount of bFGF released into the media was longitudinally measured for constructs containing 0.25% (A) or 1% (B) emulsion. A burst release of bFGF was observed (C) from the inner gel when bFGF was incorporated directly into fibrin (i.e., without emulsion). The tested masses of bFGF correspond to the bFGF loaded into the ARSs with 0.25% (167 ng) or 1% (668 ng) emulsion. The distribution of bFGF on day 2 (D) and day 8 (E) was determined by measuring the amount of bFGF released into the media as well as digesting samples of the outer gels. Data are represented as mean ± standard error of the mean (N=4-8 per condition). Statistically significant differences are denoted as follows: α: -US vs 3.3 MPa PRP, β: -US vs 8.8 MPa PRP, and γ: 3.3 MPa PRP vs 8.8 MPa PRP.

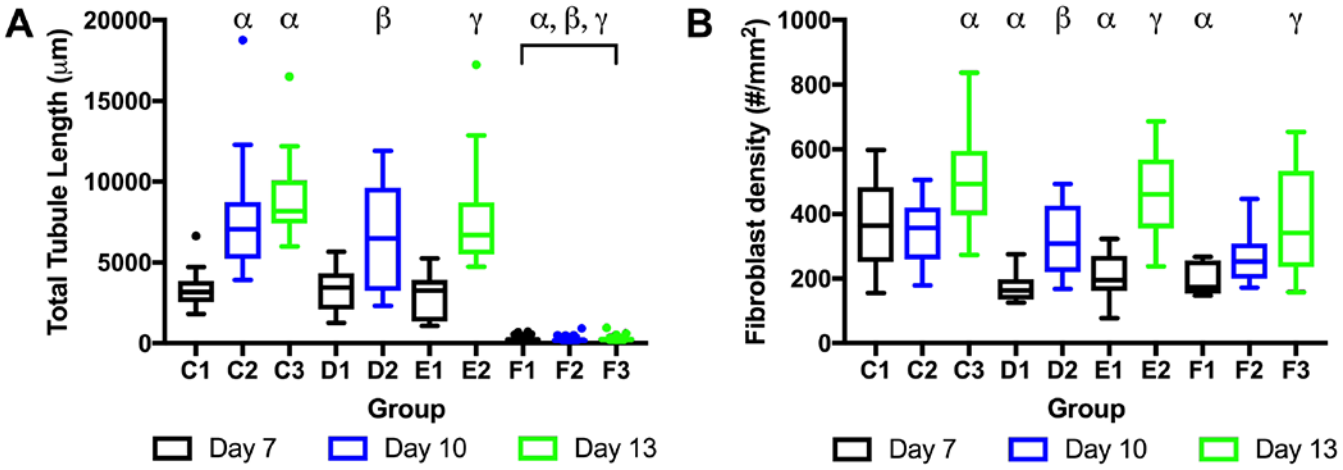

Figure 8.

The impact of the temporal presentation of bFGF on tubule length (A) and NHDF density (B) was investigated. Gel-in-gel constructs were fabricated with ARSs, containing 1% (v/v) bFGF-loaded emulsion, as the inner gels. The outer gels contained HUVEC-coated microbeads and NHDFs. The ARSs were exposed to 2.5 MHz US at 8.8 MPa PRP on day 1 according to the experimental design outlined in Table 1. Total tubule length (10 beads assessed per replicate, N=4 per condition) and NHDF density (10 views assessed per replicate, N=4 per condition) was measured at day 7, 10, or 13. Each boxed region displays the median and interquartile range (IQR) of the data. Whiskers show the range within 1.5 IQR. Statistically significant differences are denoted as follows: α: vs C1, β: vs D1, and γ: vs E1.

Table 1.

A summary of the experimental conditions interrogated during the sprouting experiments.

Cell Study	Format	Construct	Emulsion	Ultrasound
bFGF dose response	24 well	gel	N.A.	N.A.
Media controls	6 well BioFlex	gel-in-gel	N.A.	N.A.
Single US exposure	6 well BioFlex	gel-in-gel	0.25% and 1 % (v/v) blank or bFGF	3.3 or 8.8 MPa PRP
Staggered US exposure	6 well BioFlex	gel-in-gel	1% (v/v) bFGF	See Table 2

Table 2.

The impact of the temporal presentation of bFGF on angiogenic sprouting was investigated. The ARSs contained 1% (v/v) bFGF-loaded emulsion and were exposed to US at 8.8 MPa PRP at different time points. For group C, the entire ARS was exposed to US on day 1 (i.e., “complete”). For groups D and E, one half of the ARS was exposed on day 1 while the other half was exposed at a later timepoint. Groups F1-F3 were not exposed to US. Tubule length was quantified on day 7, 10, or 13.

Groups	Day 1	Day 4	Day 7	Day 10	Day 13
C1	complete		End		
C2	complete			End	
C3	complete				End
D1	1st half	2nd half	End		
D2	1st half	2nd half		End	
E1	1st half		End		
E2	1st half		2nd half		End
F1	none		End		
F2	none			End	
F3	none				End